ELSEVIER

International Journal of Heat and Fluid Flow 22 (2001) 293–300

International Journal of
HEAT AND
FLUID FLOW

www.elsevier.com/locate/ijhff

Heat transfer and flow structures in axisymmetric impinging jet controlled by vortex pairing

S.D. Hwang, C.H. Lee, H.H. Cho *

Department of Mechanical Engineering, Yonsei University, 134, Shinchon-dong, Seodaemun-gu, 120-749 Seoul, South Korea

Abstract

An experimental study is conducted to investigate the flow and heat transfer characteristics of an impinging jet controlled by vortex pairing. Two kinds of vortex control methods of secondary shear flow and acoustic excitation are applied. Local Nusselt numbers are measured on the impingement surface. Flow visualization, measurements of velocity and turbulence intensity and FFT analysis are used to understand the flow structures. The velocity ratio is changed from 0.45 to 1.75 for the shear flow control and the tested Strouhal number (excitation frequency, St_D) is 1.2, 2.4, 3.0 and 4.0 for the acoustic excitation. Enhancement or reduction in heat transfer is obtained by the control of vortex pairing due to the change of flow structures. When the vortex pairing is promoted by the secondary counter-flowing (suction flow) and $St_D = 1.2$, low heat transfer rates are obtained at large nozzle-to-plate distances. Conversely, the jet flow has an extended potential core length with the secondary co-flowing (blowing flow) and $St_D = 2.4$ and 3.0. Thus high heat transfer rates are obtained at large gap distances.

Keywords: Vortex pairing; Shear flow control; Acoustic excitation; Heat transfer coefficients; Potential core

1. Introduction

An impinging jet is a common method for heating, cooling or drying material and solid surfaces. Heat transfer under an impinging jet is generally superior to that achieved with a typical convective heat transfer method. With an impinging jet, it is easy to adjust the location of interest and to remove a large amount of heat on the impingement surface. For these reasons, the impinging jet cooling/heating technique has been widely used in many industrial systems such as cooling of high-temperature gas turbines, drying of paper or textiles, and processing of steel or glass. In recent years, it has been applied to cool high-density electrical and electronic equipment. Therefore, heat transfer and fluid flow characteristics between a single jet or multiple impinging jets and a flat surface have been the subjects of numerous investigations for many years. However, the details of the flow structures and heat transfer mechanism have not been stated clearly.

Gardon and Akfirat (1965) examined the local heat transfer coefficient on the impinging surface influenced by the turbulence from the impinging jet. Martin (1977) summarized the heat and mass transfer characteristics of impinging jets for the different nozzle types and configurations: single round nozzle, single slot nozzle, arrays of round nozzle and arrays of slot nozzle. Hoogendoorn (1977) investigated the effect of turbulence intensity of impinging circular jets on the stagnation region heat transfer for a small nozzle-to-plate distance. Goldstein and Franchett (1988) performed a study of local heat transfer characteristics of an oblique impinging jet using thermochromic-liquid crystal. Kataoka et al. (1986) showed that the heat transfer on the impingement surface was greatly enhanced with large-scale intense eddy and vortex motion. Huang and Elgenk (1994) investigated experimentally heat transfer between a uniformly heated flat plate and an impinging circular air jet to determine the values of the local and average Nusselt numbers, particularly for small values of Reynolds number and jet spacing. Jambunathan et al. (1992) and Viskanta (1993) reviewed extensively numerous studies of jet impingement heat transfer. Lytle and Webb (1994) investigated the heat transfer characteristics of a circular air impinging jet for small nozzle-to-plate spacings. The main issue about impinging jet is the enhancement of heat transfer rates or increasing of uniformity on the impingement surface by the control of jet flow. Several studies were carried out to increase the heat transfer rates of impinging jets. Zaman and Hussain (1980a,b) found that there exists a preferred mode in which the turbulence intensity of the flow is higher than that of the non-excited jet in acoustic excitation. Liu and Sullivan (1996) and Hwang et al. (2000) investigated the characteristics of acoustically excited circular impinging jets and concluded that the heat transfer rates can be increased or decreased by the change of excited frequency. For the change of nozzle exit condition and shape, Huang and El-Genk (1980) obtained more uniform heat transfer effects on the impingement surface using multi-channel swirl generators and found that the heat transfer characteristics of impinging jet are affected by the nozzle exit condition and

* Corresponding author.
E-mail address: hhcho@yonsei.ac.kr (H.H. Cho).

0142-727X/01/$ - see front matter
PII: S0142-727X(01)00091-1

Notation

A	impingement surface area (m^2)
D	nozzle exit diameter (= 24.6 mm)
f	acoustic excitation frequency (Hz)
H	nozzle-to-plate distance
h	convective heat transfer coefficient (W/m^2 K)
I	electric current (A)
k	thermal conductivity of the air (W/m K)
Nu	local Nusselt number (hD/k)
Nu_0	Nusselt number at the stagnation point
$Nu_{0,2D}$	Nusselt number of conventional jet at the stagnation point of $H/D = 2$
q_w	surface heat flux (W/m^2)
R	velocity ratio ($\Delta U/2\bar{U}$)
$\bar{R}$	gold-coated film resistance (Ω)
r	radial direction coordinate
Re_D	Reynolds number ($U_1 D/v$)
St_D	Strouhal number (fD/U_1)
T_{aw}	jet adiabatic wall temperature
T_j^0	total temperature of jet flow
T_w	wall temperature
U_1	average nozzle exit velocity of main flow
U_2	average nozzle exit velocity of secondary flow
$\bar{U}$	average velocity between main and secondary flows
ΔU	relative velocity between main and secondary flows
u	velocity of jet
u'	fluctuating velocity ($= \sqrt{u'^2}$)
x	streamwise coordinate
v	dynamic viscosity

shape. Cho et al. (1998) and Lee et al. (1998) investigated the heat transfer characteristics by the control of vortex pairing with the secondary flows for different nozzle types, such as a circular contoured nozzle and a circular pipe nozzle.

This study focuses on the changes of the flow and heat transfer characteristics in axisymmetric impinging jet controlled by vortex pairing. For this purpose, two different kinds of controlling methods are applied: one is the secondary shear flow control and the other is the acoustic excitation. The former is obtained with the additional flow (co-flowing or counter-flowing) around the main jet, and the latter is controlled by forcing the jet with the acoustic waves to the jet periphery. With the control of vortices, flow structures of impinging jets are changed, and heat transfer characteristics on the impingement plate are also affected by the change of flow structures. Flow visualization is employed to observe the growing and pairing process of vortices, and mean velocity and turbulence intensity distributions are measured by a hot-wire anemometer. Additionally, FFT (Fast Fourier Transform) is used to obtain the characteristics of vortex generation and pairing frequency. The local Nusselt numbers on the impingement surface are measured for the nozzle-to-plate spacing (H/D) of 2–16. For the shear flow control, the main and secondary flow velocity ratio (R) is changed from 0.45 to 1.75 and for the acoustic excitation, the forcing Strouhal number (excitation frequency, St_D) is 1.2, 2.4, 3.0 and 4.0. Nozzle exit Reynolds number of the main jet is fixed at 34,000 for the all tested cases, except flow visualization.

2. Experimental apparatus

Fig. 1 shows the experimental apparatus of the shear flow control and acoustic excitation systems. The main flow is supplied from a blower (3.7 kW) and passes through a heat exchanger which maintains a uniform jet temperature within ±0.2°C of the ambient temperature. The flow rates are measured using a thin plate orifice flowmeter within ±0.1% accuracy. The role of the silencer is to reduce the flow fluctuations and the sound waves which are generated at the blower. A smoothly contoured nozzle is designed to obtain a uniform velocity profile (top hat) with a large contraction ration of 50:1 (Morel, 1977). The nozzle exit diameter (D) is 24.6 mm. For the shear flow control system (Fig. 1(a)), a secondary flow nozzle has a same shape as the main nozzle and the width of the secondary flow passage is 9.4 mm (0.38D). For the acoustic excitation system (Fig. 1(b)), acoustic waves are created by a generating program (CoolEdit96) and sound card (SB32) in the PC. The sound signal is amplified by an amplifier and supplied to the woofer speaker (200 W). Sound waves generated by the woofer are supplied to a shear layer excitation device installed at the nozzle exit. The acoustic waves and signals are verified by the microphone and oscilloscope, and the sound pressure level of the excitation frequency is fixed at 95 dB.

A smoke-wire flow visualization technique is applied to understand the changes of vortex structures of the free jet using a fine nichrome wire (0.1 mm in diameter). The nichrome

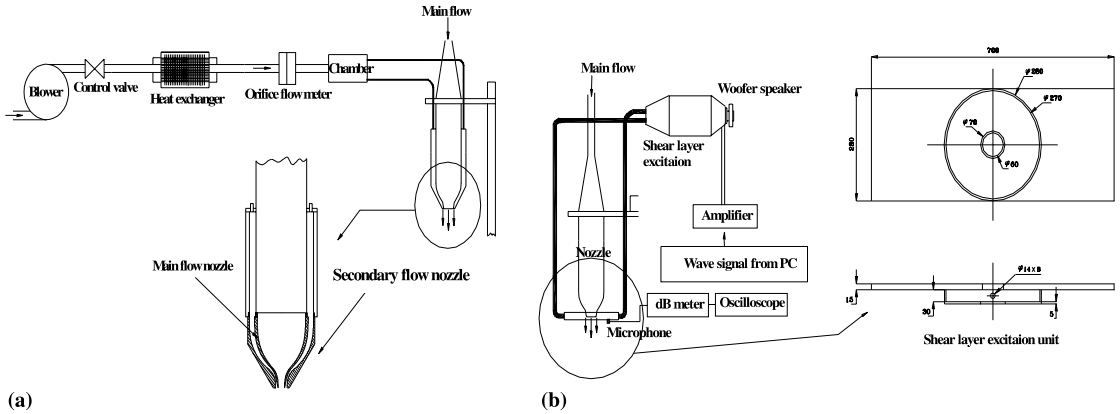

Fig. 1. Experimental apparatus for the shear flow control and acoustic excitation systems: (a) shear flow control system; (b) acoustic excitation system.

wire is located horizontally at the nozzle exit. Before each test, the wire is painted with gear oil and electric power supplies an impulse to heat the wire. Small droplets of oil distributed evenly on the wire evaporate and immediate condensation produces white smoke filament lines (streak lines). Two 500 W halogen lamps are used to produce a bright light for taking an instantaneous picture through a narrow slit.

Velocity and turbulence intensity are measured by a hot-wire anemometer (TSI-IFA300) which is a constant temperature type with I-probe sensor. A three-axis traverse controlled by the PC is used to move the hot-wire probe in the axial and radial directions. The measured data are stored in the PC through GPIB board. FFT is used to obtain frequency characteristics of the jet flow. The sampling rate is 4000 Hz and the number of sampled data is 4096 points, and a LPF (low pass filter) of 2000 Hz is used for all these procedures.

Local surface temperature or heat transfer coefficients on the impingement surface are measured by the thermocouples (T-type) under a constant heat flux condition. The test plate includes a gold-coated film (Aure-12) bonded on a thin laminate plate of 5 mm in thickness using a double-sided adhesive tape. The laminate plate is insulated with a 50 mm Styrofoam and a 50 mm thick fiberglass. In order to obtain a constant heat flux condition, two large copper bus bars, placed at each end of the gold-coated film, are connected to the power supply through a voltage trap (shunt) to measure the current. Thirty-five thermocouples (36-gauge copper-constantan type) are embedded in the laminate plate beneath the gold-coated film with a spacing of $0.2D$ in the radial direction. Thermal epoxy (copper oxide) is used as a filling cement and an electrical insulator for the gold-coated film. The temperature measuring system consists of a switching system (Keithley model 7001), a multimeter (Keithley model 2001) and a personal computer.

The convective heat transfer coefficient is defined by

$$h = \frac{q_w}{T_w - T_{aw}}, \tag{1}$$

where q_w is the heat flux from the surface, T_w is the wall temperature, and T_{aw} is the jet adiabatic wall temperature. Since the flow velocity of the jet is slow, the adiabatic wall temperature (T_{aw}) is nearly equally to the jet total temperature (T_j^0), measured in the plenum (about 0.4 m/s) positioned 450 mm upstream of the jet nozzle exit (where $U_1 = 20$ m/s, dynamic temperature $\cong 0.2$°C) . Therefore, the local heat transfer coefficient can be written by

$$h = \frac{q_w}{T_w - T_j^0} \tag{2}$$

and q_w is obtained as

$$q_w = I^2 \frac{\bar{R}}{A}, \tag{3}$$

where I is the electric current in the gold-coated film, $\bar{R}$ is the overall resistance, and A is the area of the impingement surface. The jet temperature is maintained within ± 0.2°C of the ambient temperature, so that the entrainment effects of the ambient air (due to the temperature difference) are neglected in the present study. The heat conduction loss through the insulation material is negligible because of the low-thermal conductivity and large thickness of the insulation material. The radiation heat loss is also neglected since the present experiment is conducted with the surface temperature held below 50°C. The electric current is controlled by a variable power supply and measured precisely using a shunt within $\pm 1.0\%$ accuracy.

Experimental results for heat transfer are presented in terms of the Nusselt number

$$Nu = \frac{hD}{k} = \frac{q_w}{T_w - T_j^0} \frac{D}{k}, \tag{4}$$

where k is the conductivity of the jet air. Using a methodology outlined by Kline and McClintock (1953), the uncertainty in the 95% confidence level is about 3% in the Nusselt number.

3. Results and discussion

3.1. Shear flow control

3.1.1. Flow characteristics with the secondary flows

The velocity ratio, R, is defined by

$$R = \frac{\Delta U}{2\bar{U}} = \frac{U_1 - U_2}{U_1 + U_2} \tag{5}$$

and it is used to present data as a flow parameter. U_1 and U_2 are the nozzle exit velocity of main and secondary flow, respectively. The velocity difference, ΔU, describes an intensity of the shear across the mixing layer and the average velocity, $\bar{U}$, is the average speed of the mixing layer. Consequently, $R < 1.0$ means co-flowing and $R > 1.0$ means counter-flowing. If there is no secondary flow around the main jet, R is equal to 1.0.

The flow patterns with secondary flows are shown in Fig. 2. For the free jet without secondary flow ($R = 1.0$), a ring vortex, created around the jet by the virtue of the instability of the mixing layer, moves downstream. As the vortex moves downstream, it undergoes a process of pairing and development. When the vortex generated at the mixing layer grows in size, it affects the core of the jet flow and finally the potential core disappears. For the co-blowing flow of $R = 0.45$, there are two shear layers between the main jet and the ambient air because the secondary flow is ejected around the main jet. One is the shear layer between the secondary flow and the ambient air and the other is between the main flow and the secondary flow. The

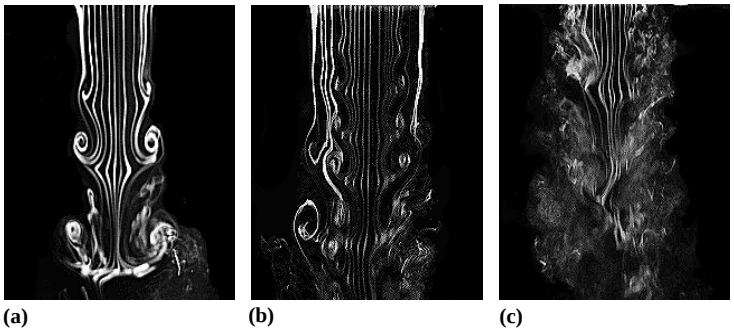

Fig. 2. Flow visualization results of free jet with the secondary flows ($Re_D = 3400$): (a) $R = 1.0$; (b) $R = 0.45$; (c) $R = 1.45$.

development of the main jet flow is delayed by the secondary blowing flow. The reason is that the co-rotating outer vortices inhibit vortex pairings of the inner vortices and the entrainment of ambient air. As a result, the jet potential core extends far downstream. For the suction case of $R = 1.45$, there are also two shear layers, but the characteristics of the vortices are different from those of $R = 1.0$ or 0.45. With the suction flow, development of the main jet is promoted because of the relatively high shear between the main and secondary flows.

Fig. 3 shows the variation of velocity and turbulence intensity distributions measured along the centerline of the main jet with the secondary flows. In the case of conventional jet ($R = 1.0$), the flow maintains uniform nozzle exit velocity (potential core) for a distance of $4 \sim 5D$. As the flow is de-

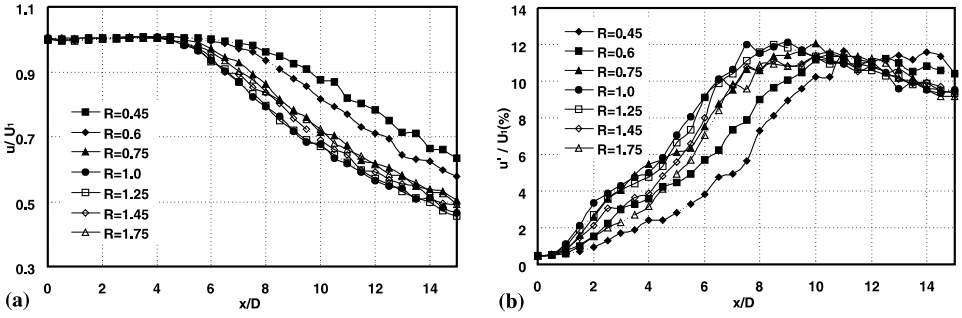

Fig. 3. Effect of R on velocity and turbulence intensity distributions along the centerline of the free jet ($Re_D = 34,000$): (a) velocity; (b) turbulence intensity.

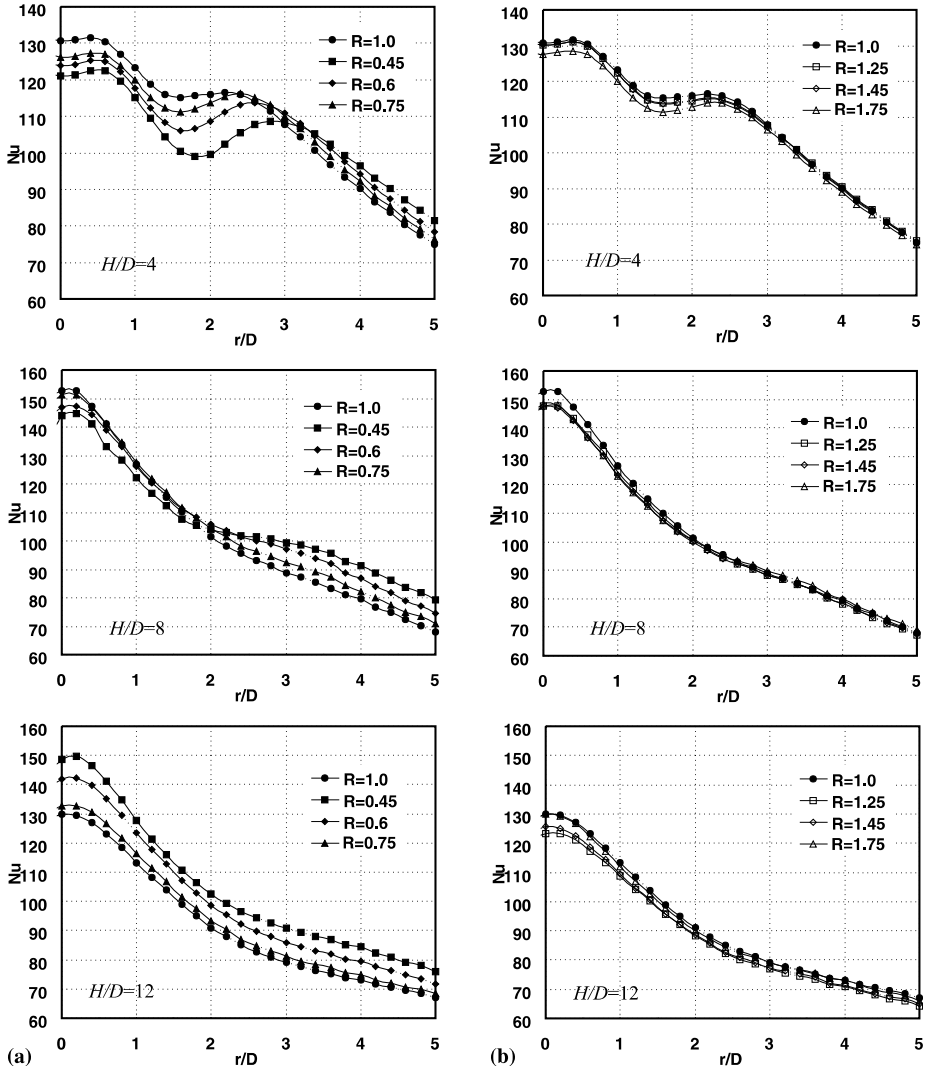

Fig. 4. Effects of H/D and R on radial distribution of Nu ($Re_D = 34,000$): (a) co-flowing; (b) counter-flowing.

veloping and the vortices are growing, the velocity of the jet decreases monotonically. The turbulence intensity is low at the nozzle exit and increases steadily until $x/D \cong 8$. When the jet flow is fully developed, the turbulence intensity decreases slowly. In the case of co-flowing ($R < 1.0$), the potential core length is longer than that of the conventional jet and the turbulence intensity is very low. As shown in the flow visualization results, the secondary blowing inhibits vortex pairings and flow entrainment of the ambient air. Hence, the development of the jet flow is delayed by the secondary blowing flow. However, the suction flow ($R > 1.0$) reduces the potential core length and increases the turbulence intensity at the center of the jet. The reason is that the suction flow promotes the flow development as shown in the flow visualization results.

3.1.2. Heat transfer characteristics with the secondary flows

Fig. 4 shows the effects of H/D and R on the radial distribution of Nu. The conventional impinging jet shows some distinct heat transfer characteristics on the impingement surface. For a small nozzle-to-plate spacing ($H/D = 4$), there exist two local peaks. The first peak at $r/D \cong 0.5$ is caused by the effect of stagnation flow acceleration. The flow acceleration reduces the boundary layer thickness resulting in the heat transfer increase. The secondary peak appears at $r/D \cong 2.1$. Generally, it is considered that the secondary peak in Nu is induced by the flow transition from laminar to turbulence and by the secondary vortices generated at $r/D \cong 2$. The vortices near the wall disturb the boundary layer flow and enhance the mixing of ambient fluids, creating the peak value of Nu. As the gap distance increases ($H/D = 12$) and the impingement plate is located outside of the jet potential core, there is only one peak at the stagnation point. This is because the jet flow is fully developed and the turbulence intensity at the stagnation region is sufficiently high, as shown in the flow characteristics of free jet. For the blowing case, Fig. 4(a) shows somewhat different characteristics in Nu distributions even though the trend is similar. For small gap distance ($H/D = 4$), there also exist two peaks, but the Nu at the stagnation point is low due to the lower turbulence intensity of the jet core flow with the secondary blowing flow. The position of the secondary peak is shifted downstream. This is considered to be caused by the delay of transition to turbulence due to the low turbulence intensity. High heat transfer rates with the secondary blowing are obtained as the spacing increases ($H/D = 12$) because the jet core velocity is relatively high and the flow has a longer jet potential core length. Nu increases as the blowing velocity increases (as the velocity ratio R decreases). For the suction flow (Fig. 4(b)), the heat transfer coefficients are insensitive to the suction flows at $H/D = 4$. This is because the impingement plate is within the potential core region. Conversely, at a large nozzle-to-plate distance of $H/D = 12$, Nu is slightly lower than that of the conventional jet due to the lower velocity in the jet core region.

Nu at the stagnation point for various H/D are shown in Fig. 5. As mentioned above, for the secondary blowing cases (Fig. 5(a)), the Nusselt number for the small spacing is slightly lower than that of the conventional jet. As the distance increases, this trend is reversed and higher heat transfer rates are obtained. For the suction cases, the Nusselt numbers are little different at the small nozzle-to-plate distances ($H/D \leqslant 4$) but they shows some difference as increasing nozzle-to-plate distances.

3.2. Acoustic excitation

3.2.1. FFT

The Strouhal number St_D indicates the frequency characteristics of the flow and is defined by

$$St_D = \frac{fD}{U_1}, \tag{6}$$

where f is the forcing frequency of the acoustic excitation or generating vortex frequency. $St_D = 0$ means the conventional jet without acoustic excitation.

FFT using a hot-wire anemometer is used to analyze the frequency characteristics of vortex formation and pairing. Fig. 6 shows the FFT results of free jet with the acoustic excitation. In the case of conventional jet ($St_D = 0$), there are two distinguishing frequencies at $x/D = 1.0$ as shown in Fig. 6(a). One is the frequency of about 1000 Hz ($St_D \cong 1.2$) which is related to the fundamental frequency of vortex generation. The other is about 500 Hz ($St_D \cong 0.6$) due to vortex pairing. The fundamental frequency (1,000 Hz) is a peculiar frequency of vortex generation produced by the initial instability of jet flow. When the vortices are convected downstream, two vortices join together (vortex pairing) resulting in the half frequency characteristic (500 Hz) of fundamental frequency. As the flow is convected downstream, the amplitude of the power spectral density increases and only one dominant frequency is shown due to the pairing of vortices. At $x/D = 6$, the dominant frequency disappears and uniform frequency distributions are shown for the all frequency range.

When the flow is excited with the frequency of $St_D = 2.4$ ($f = 1950$ Hz), there are two clear peak frequencies at $x/D = 1.0$. The vortices (fundamental frequency, $St_D = 1.2$) are reinforced by the excitation, so that the dominant frequencies are maintained far downstream. The reason is that the excitation frequency suppresses the vortex pairing. When the flow is excited with a frequency of $St_D = 3.0$ ($f = 2440$ Hz), the dominant frequency of jet vortices occurs at about 1200 Hz ($St_D \cong 1.5$) and it is a little higher than that of the non-excited jet. For the excitation frequency of $St_D = 4.0$ ($f = 3250$ Hz), Fig. 6(d) shows similar trends to the conventional jet. The results show that the frequency characteristics of jet flow are affected strongly by the acoustic excitation. However, the vortex frequencies of the jet flows are not directly related to the

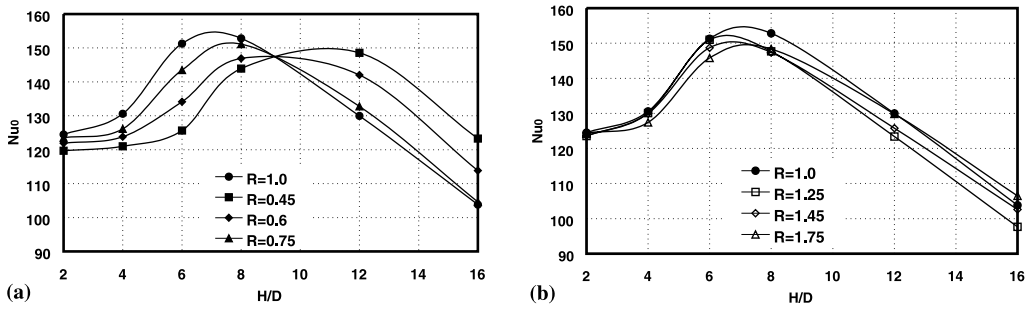

Fig. 5. Effect of R on variation of Nu at the stagnation point with various H/D ($Re_D = 34,000$): (a) blowing; (b) suction.

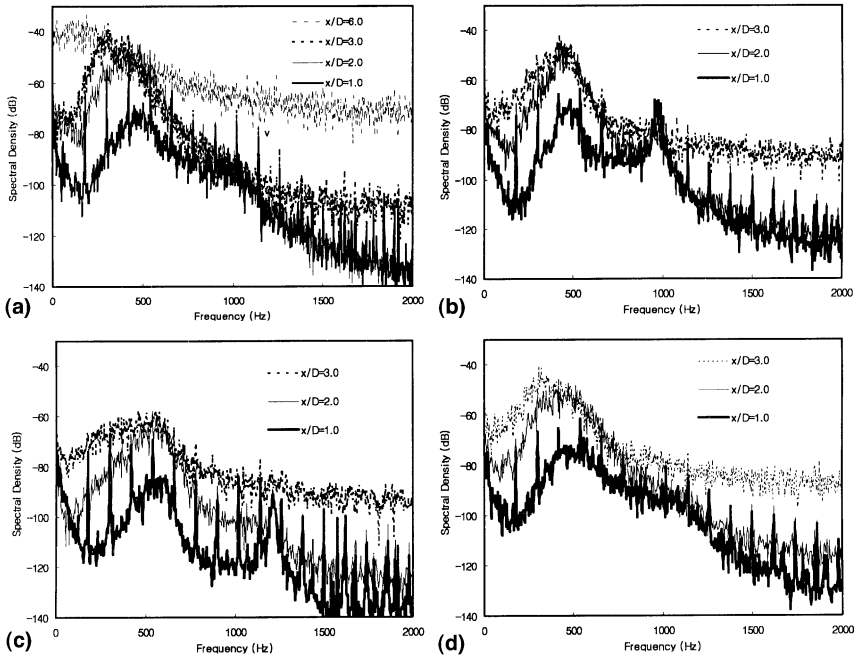

Fig. 6. Power spectral density of free jet with acoustic excitation ($Re_D = 34,000$): (a) $St_D = 0$; (b) $St_D = 2.4$; (c) $St_D = 3.0$; (d) $St_D = 4.0$.

excitation frequency itself. The subharmonic frequency of the excitation frequency has an important role to the control of vortex generation and pairing.

3.2.2. Flow characteristics with acoustic excitation

Fig. 7 shows the flow visualization results of free jet with the acoustic excitations. For the case of $St_D = 1.2$, the vortices generated at the nozzle exit by the initial instability of jet flow are not clearly shown and breaks down quickly due to the promotion of vortex pairing. When the excitation frequency, St_D, is 2.4, the vortices around the jet periphery do not develop and maintain their shape and size downstream. The flow excited by the frequency of $St_D = 3.0$ presents a similar tendency to the case of $St_D = 2.4$. The vortices formed at the nozzle exit by the instability are strengthened and the vortex pairing and development is suppressed with the acoustic excitation at the

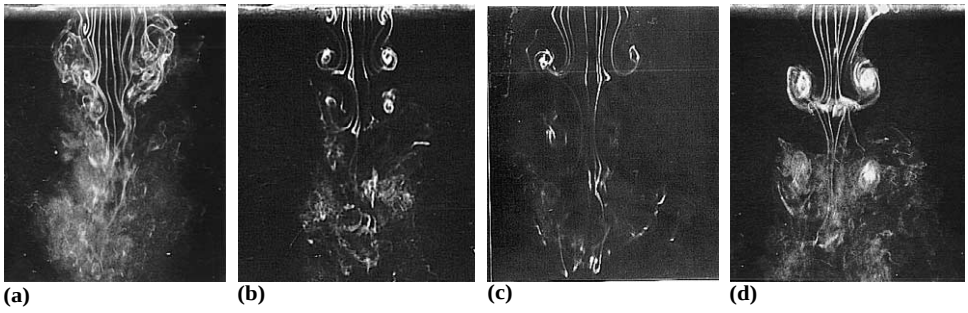

Fig. 7. Flow visualization results of free jet with acoustic excitation ($Re_D = 3400$): (a) $St_D = 1.2$; (b) $St_D = 2.4$; (c) $St_D = 3.0$; (d) $St_D = 4.0$.

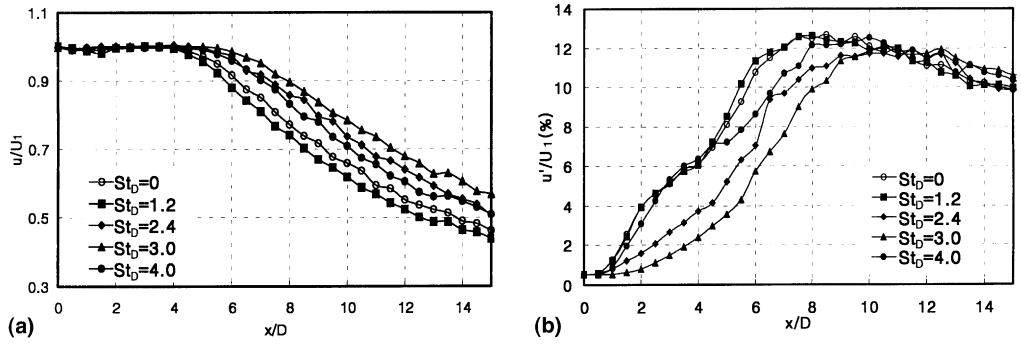

Fig. 8. Effect of St_D on velocity and turbulence intensity along the centerline of free jet ($Re_D = 34,000$): (a) velocity; (b) turbulence intensity.

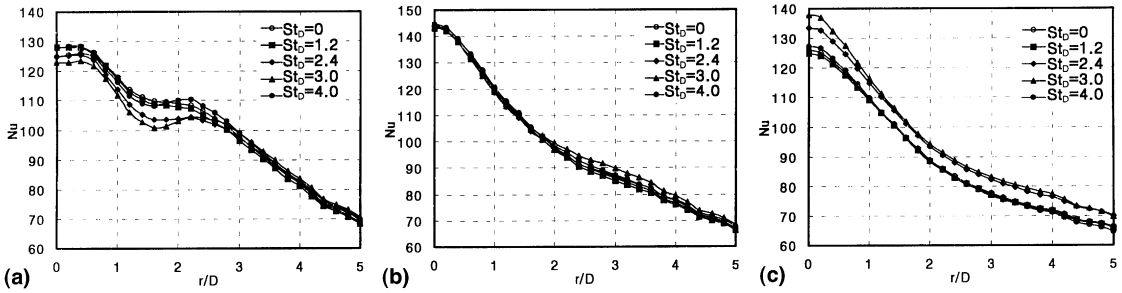

Fig. 9. Effects of H/D and St_D on radial distribution of Nu ($Re_D = 34,000$): (a) $H/D = 4$; (b) $H/D = 8$; (c) $H/D = 12$.

frequency of $St_D = 2.4$ and 3.0. Hence, the vortices convect far downstream, maintaining their size. For the case of $St_D = 4.0$, the vortices grow rapidly in size and develop by the promotion of vortex pairing. The flow visualization results are reasonably consistent with the FFT results.

Fig. 8 presents the velocity and turbulence intensity distributions along the centerline of the free jet with the acoustic excitations. The characteristics of the non-excited jet are explained by the flow characteristics of the conventional jet. With acoustic excitation, the general trends of the velocity distributions are similar to the non-excited jet, but the jet potential core lengths change significantly. When the vortex pairing and development of the jet are suppressed by the acoustic excitation frequency of $St_D = 2.4$ and 3.0, the potential core length is longer than that of the non-excited jet and the turbulence intensity increases slowly, resulting in lower values within the potential core region. In the case of $St_D = 1.2$, the jet flow has a lower velocity and a higher turbulence intensity due to the promotion of vortex pairing and jet flow development. When the jet flows are fully developed, for $x/D \geqslant 10$, turbulence intensities are similar for all tested cases.

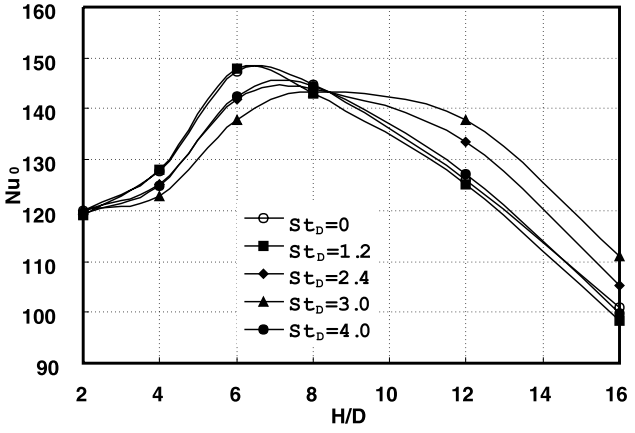

Fig. 10. Effect of St_D on variation of Nu at stagnation point with H/D ($Re_D = 34,000$).

3.2.3. Heat transfer characteristics with acoustic excitation

Fig. 9 presents Nu for various nozzle-to-plate distances and acoustic excitations. When H/D is 4 and the excitation frequency, St_D, is 2.4 and 3.0, heat transfer rates at the stagnation point are lower than those of the non-excited jet. The position of the secondary peak of the Nusselt number moves outward in the radial direction, like the blowing case, due to the delay of the flow transition and low turbulence intensity. For the case of $St_D = 1.2$, Nu are little different from the non-excited jet. At the large gap distance ($H/D = 12$), the high heat transfer rates are obtained with the excited frequency of $St_D = 2.4$ and 3.0. However, Nu at the stagnation point for $St_D = 1.2$ is slightly lower than that of the non-excited jet.

Fig. 10 shows Nu at the stagnation point with different acoustic excitations. For small spacings, the Nu with $St_D = 2.4$ and 3.0 is lower than that of the non-excited jet due to the low turbulence intensity. As the gap distance increases, high heat transfer rates are obtained with the excitation frequency of $St_D = 2.4$ and 3.0 as a result of the longer potential core length. For the case of $St_D = 1.2$, the Nusselt number distributions are similar to those of the non-excited jet at the small gap distance and are a little lower than that of the non-excited jet at the large nozzle-to-plate distance of $H/D = 16$ because the jet flow has relatively low velocity. For the case of $St_D = 4.0$, the heat transfer trend at the stagnation point is similar to the case of $St_D = 1.2$ and the non-excited jet.

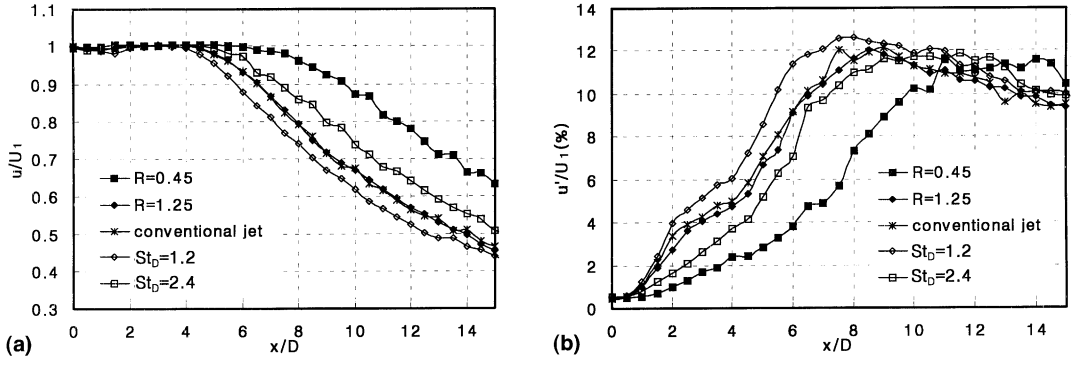

Fig. 11. Comparison of velocity and turbulence intensity with secondary flows and acoustic excitation ($Re_D = 34,000$): (a) velocity; (b) turbulence intensity.

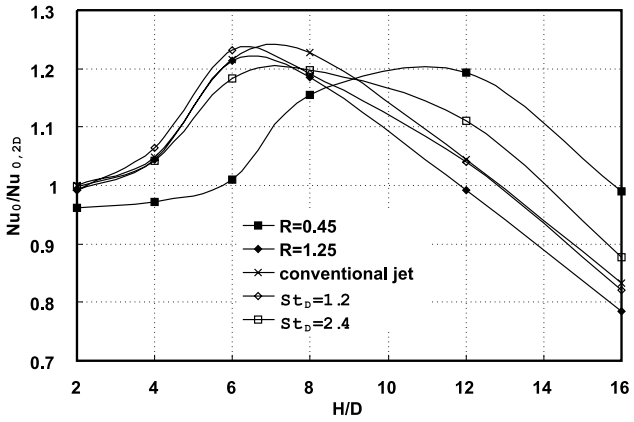

Fig. 12. Comparison of Nu at the stagnation point with secondary flows and acoustic excitations ($Re_D = 34,000$).

3.3. Comparison of secondary flow and acoustic excitation

Fig. 11 shows the variation of the velocity and turbulence intensity distributions with the secondary flows and the acoustic excitation. By the promotion of vortex pairing with the suction flow of $R = 1.25$ and acoustic excitation of $St_D = 1.2$, relatively low velocity and high turbulence intensity is obtained. However, for the blowing of $R = 0.45$ and the excitation frequency of $St_D = 2.4$ and 3.0, high velocity (longer potential core length than that of the conventional jet) and low turbulence intensity are obtained due to the suppression of vortex pairing and jet flow development.

Fig. 12 presents the comparison of Nu at the stagnation point with the secondary flows and the acoustic excitations. These results represent the changes in heat transfer characteristics of impinging jet due to the control of vortex pairing. When the flow development is promoted by the suction flow or $St_D = 1.2$, the flow has slightly higher turbulence intensity and lower velocity than that of the conventional jet. Therefore, low heat transfer rates are obtained at the large gap distance. On the other hand, high heat transfer rates are obtained at large gap distances due to the extended jet potential core length with the blowing flow or $St_D = 2.4$ and 3.0.

4. Conclusion

Flow structures of jets are affected strongly by the nozzle exit conditions and vortices generated around the jet periphery. Hence, the flow characteristics of impinging jet are changed largely by the control of vortex pairing. For the jet flow forced by the suction or the acoustic excitation of $St_D = 1.2$, the jet flow has a shorter potential core length and slightly higher turbulence intensity. In the case of blowing or $St_D = 2.4$ and 3.0, the vortex pairing is suppressed and the development of jet flow is delayed. As a result, the jet has a longer potential core length and lower turbulence intensity within the jet core region.

Heat transfer characteristics on the impingement surface are affected by the change of jet flow structures. As the development of jet flows is promoted by the suction flow or the acoustic excitation of $St_D = 1.2$, heat transfer rates are enhanced a little at small gap distances with high turbulence intensity. However, the heat transfer rates are slightly lower at the large gap distances due to the lower jet stream velocity. Conversely, the heat transfer rates are reduced a little at short gap distances and formation of the secondary peak of heat transfer coefficients is delayed due to the low turbulence intensity of the jet core flow controlled by the secondary blowing flow or $St_D = 2.4$ and 3.0. Enhancement in heat transfer rates are obtained at large gap distances by the suppression of vortex pairing and development of the jet resulting in extended potential core length with secondary blowing flow or $St_D = 2.4$ and 3.0.

Acknowledgements

This work was supported by the National Research Laboratory program of Korea Institute of Science and Technology Evaluation and Planning.

References

Cho, H.H., Lee, C.H., Kim, Y.S., 1998. Characteristics of heat transfer in impinging jets by control of vortex pairing. ASME paper No. 98-GT-276.

Gardon, R., Akfirat, J.C., 1965. The role of turbulence in determining the heat transfer characteristics of impinging jets. Int. J. Heat and Mass Transfer 8, 1261–1272.

Goldstein, R.J., Franchett, M.E., 1988. Heat Transfer from a flat surface to an oblique impinging jet. J. Heat Transfer 110, 84–90.

Hoogendoorn, C.J., 1977. The effect of turbulence on heat transfer at a stagnation point. Int. J. Heat and Mass Transfer 20, 1333–1338.

Huang, L.M., Elgenk, M.S., 1994. Heat-transfer of an impinging jet on a flat surface. Int. J. Heat and Mass Transfer 37, 1915–1923.

Huang, L., El-Genk, M.S., 1980. Heat transfer and flow visualization experiments of swirling, multi-channel and conventional impinging jets. Int. J. Heat and Mass Transfer 41, 583–600.

Hwang, S.D., Lee, C.H., Cho, H.H., 2000. Heat transfer characteristics on impingement surface with control of axisymmetric jet(2) - with acoustic excitation. Trans. KSME(B) 24, 373–381.

Jambunathan, K., Lai, E., Moss, M.A., Button, B.L., 1992. A review of heat transfer data for single circular jet impingement. Int. J. Heat and Fluid Flow 13, 106–115.

Kataoka, K., Mihata, L., Maruo, K., Suguro, M., Chiguesa, T., 1986. Quasi-periodic large-scale structure responsible for the selective enhancement of impinging jet heat transfer. Proc. Eighth IHTC 3, 1193–1198.

Kline, S.J., McClintock, F.A., 1953. Describing uncertainties in single sample experiments. Mech. Eng. 75, 3–8.

Lee, C.H., Kim, Y.S., Cho, H.H., 1998. Heat transfer characteristics on impingement surface with control of axisymmetric Jet(1) - uniform velocity distribution jet. Trans of KSME(B) 22, 386–398.

Liu, T., Sullivan, J.P., 1996. Heat transfer and flow structures in an excited circular impinging jet. Int. J. Heat and Mass Transfer 39, 3695–3706.

Lytle, D., Webb, B.W., 1994. Air jet impingement heat transfer at low nozzle-plate spacings. Int. J. Heat and Mass Transfer 37, 1687–1697.

Martin, H., 1977. Heat and mass transfer between impinging gas jets and solid surfaces. Adv. Heat Transfer 13, 1–60.

Morel, T., 1977. Design of two-dimensional wind tunnel contractions. J. Fluids Eng. 99, 371–378.

Viskanta, R., 1993. Heat transfer to impinging isothermal gas and flamejets. Experiment. Therm. and Fluid Sci. 6, 111–134.

Zaman, K.B.M., Hussain, A.K.M.F., 1980a. Vortex pairing in a circular jet under controlled excitation. Part 1. General jet response. J. Fluid Mech. 101, 449–491.

Zaman, K.B.M., Hussain, A.K.M.F., 1980b. Vortex pairing in a circular jet under controlled excitation. Part 2. Coherent structure dynamics. J. Fluid Mech. 101, 493–544.